

# Widespread moulin formation during supraglacial lake drainages in Greenland

Matthew J. Hoffman<sup>1</sup>, Mauro Perego<sup>2</sup>, Lauren C. Andrews<sup>3</sup>, Stephen F. Price<sup>1</sup>, Thomas A. Neumann<sup>4</sup>, Jesse Johnson<sup>5</sup>, Ginny Catania<sup>6,7</sup>, Martin Lüthi<sup>8</sup>

<sup>1</sup>Fluid Dynamics and Solid Mechanics Group, Los Alamos National Laboratory

<sup>2</sup>Center for Computing Research, Sandia National Laboratories

<sup>3</sup>Global Modeling and Assimilation Office, NASA Goddard Space Flight Center

<sup>4</sup>Cryospheric Sciences Laboratory, NASA Goddard Space Flight Center

<sup>5</sup>Department of Computer Science, University of Montana

<sup>6</sup>Institute for Geophysics, University of Texas

<sup>7</sup>Department of Geological Sciences, University of Texas

<sup>8</sup>Department of Geography, University of Zürich

## Key Points:

- Ice sheet model inversion using ice velocity from 11 station GPS network reveals Greenland ice sheet surface stresses at hourly resolution.
- Conditions for fracturing and moulin formation expand slightly in spring and summer but substantially during brief lake drainage event.
- Most mapped moulins could form only during large ice stresses associated with supraglacial lake drainages.

## Abstract

Moulins permit access of surface meltwater to the glacier bed, causing basal lubrication and ice speedup in the ablation zone of western Greenland during summer. Despite the substantial impact of moulins on ice dynamics, the conditions under which they form are poorly understood. We assimilate a time-series of ice surface velocity from a network of eleven Global Positioning System receivers into an ice sheet model to estimate ice sheet stresses during winter, spring, and summer in a  $\sim 30 \times 10$  km region. Surface-parallel von Mises stress increases slightly during spring speedup and early summer, sufficient to allow formation of 16% of moulins mapped in the study area. In contrast, 63% of moulins experience stresses over the tensile strength of ice during a short (hours) supraglacial lake drainage event. Lake drainages appear to control moulin density, which is itself a control on subglacial drainage efficiency and summer ice velocities.

## 1 Introduction

In the ablation zone of the Greenland Ice Sheet surface meltwater drains to the bed during summer, causing speedup of ice flow due to pressurization of the subglacial drainage system [e.g., Zwally *et al.*, 2002; Bartholomew *et al.*, 2010; Hoffman *et al.*, 2011]. However, the supraglacial hydrologic system and its englacial connection to the subglacial drainage system has substantial complexity that is not fully understood [McGrath *et al.*, 2011; Banwell *et al.*, 2012; Arnold *et al.*, 2014; Clason *et al.*, 2015; Smith *et al.*, 2015; Banwell *et al.*, 2016; Yang and Smith, 2016]. Beyond the marginal few kilometers, all surface melt finds its way into the Greenland ice sheet, with a large fraction conveyed by supraglacial streams that terminate in moulins draining to the bed, and the remainder draining into crevasses [McGrath *et al.*, 2011; Clason *et al.*, 2015; Smith *et al.*, 2015; Yang and Smith, 2016; Koziol *et al.*, 2017]. Theory, observations, and modeling indicate that the existence and spatial distribution of these surface-to-bed connections have a strong control on the evolution of the basal drainage system and its associated impact on ice dynamics [Gulley *et al.*, 2012; Banwell *et al.*, 2016].

Because of cold interior ice in Greenland [ $\sim -10$  to  $-20^\circ\text{C}$ , e.g., Lüthi *et al.*, 2015, for our study area], the primary surface-to-bed connections are moulins formed through “hydrofracture” [Das *et al.*, 2008; Doyle *et al.*, 2013; Tedesco *et al.*, 2013; Carmichael *et al.*, 2015; Stevens *et al.*, 2015]. Hydrofracture requires an ample supply of water and can occur where fractures are fed by, or form beneath, supraglacial lakes (Figure 1a) or supraglacial streams (Figure 1b,c). In this process, water, having greater density than ice, deepens pre-existing fractures in the ice surface, potentially rapidly (hours) to the bed if sufficient supply of water is maintained [van der Veen, 2007; Krawczynski *et al.*, 2009; Tsai and Rice, 2010], or slowly (days) if the water supply is limited [Boon and Sharp, 2003]. While substantial amounts of surface melt also drain into crevasse fields [McGrath *et al.*, 2011; Clason *et al.*, 2015; Smith *et al.*, 2015; Yang and Smith, 2016; Koziol *et al.*, 2017], the cold thermal barrier existing through much of the ice column in west Greenland appears to prevent the formation of an extensive englacial system [Lüthi *et al.*, 2015; Poinar *et al.*, 2017]; moulins can exist within crevasse fields but are fundamentally similar to moulins formed elsewhere. Once moulins form, they can become persistent features maintained for multiple years if they continue to receive a regular supply of water from supraglacial runoff [Catania *et al.*, 2008; Catania and Neumann, 2010], suggesting moulin formation events have a long-lived impact on the hydrology, and, in turn, the seasonal dynamics, of the ice sheet.

Moulin formation during supraglacial lake drainage has been well-documented [e.g., Boon and Sharp, 2003; Das *et al.*, 2008; Doyle *et al.*, 2013; Stevens *et al.*, 2015], but the controls on rapid lake drainage initiation in Greenland remain unknown. In the one event where the cause has been clearly elucidated, the lake drainage was not spontaneous but triggered by uplift and tension caused by meltwater reaching the bed through preexisting

englacial connections nearby [Stevens *et al.*, 2015]. The triggering event resulted in local ice acceleration and a change in the stress regime of the surrounding area that caused temporary fracturing beneath the lake. Lakes expanding to encompass an existing crevasse or moulin is an alternate mechanism, which may be initiated by rapid filling of a lake from runoff or overflow of a lake upstream [Tedesco *et al.*, 2013]. Despite the well understood formation of moulins associated with supraglacial lake drainage and crevasse fields, many moulins are located kilometers from both supraglacial lakes and crevasse fields (Figure 1b,c) [Phillips *et al.*, 2011; Lampkin and Vanderberg, 2014; Smith *et al.*, 2015; Yang and Smith, 2016]. These moulins drain a substantial part of the ice surface [Lampkin and Vanderberg, 2014; Smith *et al.*, 2015; Koziol *et al.*, 2017], yet have no clear mechanism of formation.

Here, we investigate conditions under which moulins form in west Greenland by comparing modeled ice stresses to satellite observations of crevasse and moulin locations. We extend previously used methods of estimating the tensile strength of glacier ice from observed crevasse extent [Vaughan, 1993; Clason *et al.*, 2015; Colgan *et al.*, 2016; Koziol *et al.*, 2017] to evaluate how moulins open in the same area, uniquely considering hourly stress variations during the dynamic Greenland summer. To do so, we use an ice sheet model optimization framework at half kilometer resolution to assimilate point observations of ice velocity from Global Positioning System (GPS) measurements. The GPS-derived velocity records provide subdaily temporal resolution of the ice sheet stress state and its affect on fracture formation. Moulins are assumed to occur where sufficient surface melt-water exists in summer to drive hydrofracture to the bed. Comparing modeled stresses from winter, spring, and summer, we infer that moulins are most likely to form during the much larger stresses that occur during a short-lived supraglacial drainage event.

## 2 Study Area and Methods

Our study area in the ablation zone of west Greenland extends approximately 30 km along a flowline and 10 km laterally (Figure 2). The area is between 15 and 45 km upstream of the terminus of the outlet glacier Sermeq Avannarleq and was the site of a number of previous studies, including a borehole drilling campaign [Andrews *et al.*, 2014; Ryser *et al.*, 2014a,b; Walter *et al.*, 2014; Lüthi *et al.*, 2015; Rösli *et al.*, 2016; Hoffman *et al.*, 2016]. Ice thickness varies between 500 and 1000 m in the region, and winter ice speed ranges between about 60 and 180 m a<sup>-1</sup>.

### 2.1 Satellite Image Analysis

Locations of crevasse fields and moulins in the study area were digitized manually from WorldView-1 and WorldView-2 0.6 m resolution panchromatic satellite imagery. Digitization of crevasses was performed at a scale of 1:2,500. Because illumination and snow cover was not optimal in all images used and to allow for the possibility of changes in crevasse extent, the digitization of crevasses was repeated for three years (2009–2011). To ensure we consider crevasse fields related to the background winter stress field, we defined persistent crevasse fields as the extent that is common to all three years (Supporting Figure 2, Figure 2).

To create a moulin position dataset for 2011, moulin locations were identified manually in WorldView-2 imagery at a resolution of 1:3,000, primarily through the identification of abrupt supraglacial stream termination. We also used the presence of refrozen spray downstream of a hole or fracture in the ice and evidence of supraglacial lake drainage. Where images overlap, moulins were identified in the most recent image. We estimated the moulin positional uncertainty to be approximately 24 m for the 2011 dataset. We categorized moulins associated with rapid lake drainage as those within 500 m of a rapid lake drainage location in the inventory of Morriss *et al.* [2013], which identified any lake that drained rapidly (within 6 days) in one or more years during the 2002–2011 period. The

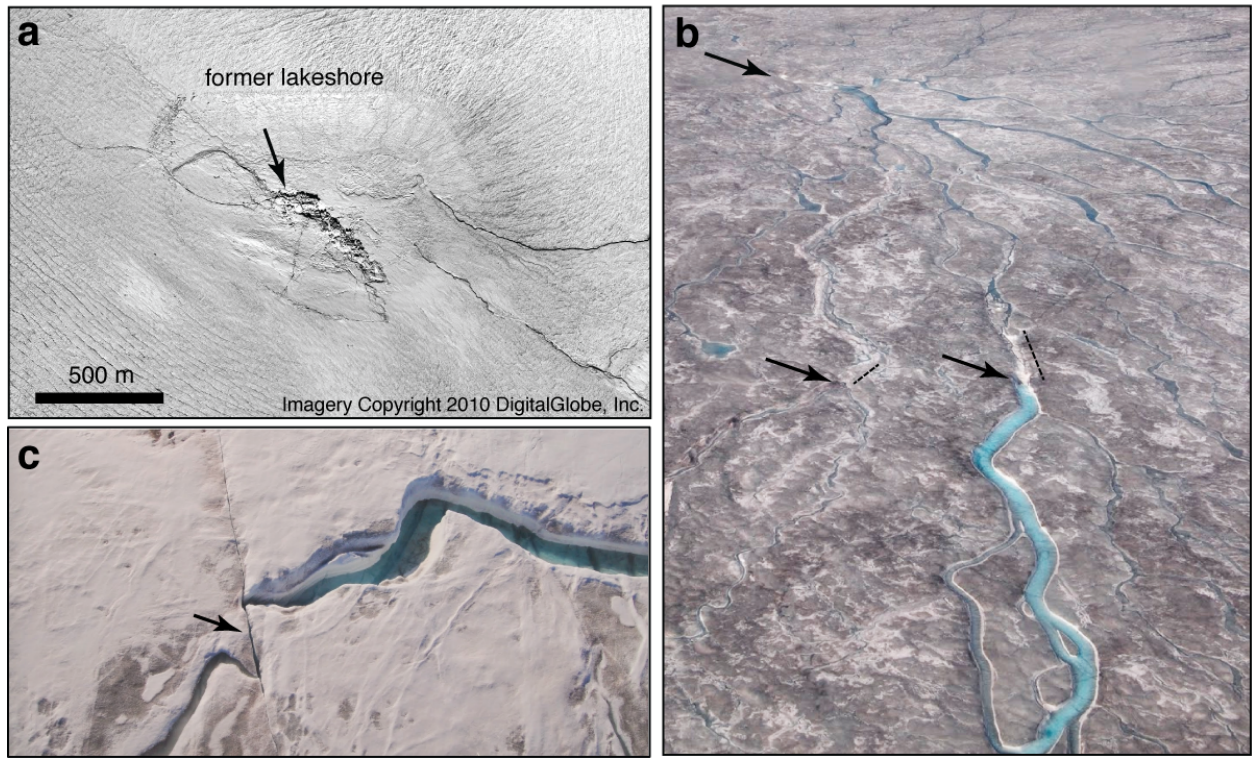


**Figure 1.** Examples of moulins within the study area. a) WorldView satellite photo of moulin formed within supraglacial lake basin. The former lakeshore can be seen as an oval “bathtub ring” in the center of the photograph. Upthrust blocks of ice can be seen around the primary moulin in the center of the image (indicated with an arrow), and long fractures extend out of the lake basin to the left, the right, and the lower right. A crevasse field covers the lower left of the image but does not intersect the lake basin. This lake is located at  $69.45^{\circ}\text{N}$   $49.63^{\circ}\text{W}$ . b) Aerial photograph of streams terminating in moulins (black arrows) without any nearby visible fractures or lakes. The flow direction of the major streams is from the bottom of the photo toward the top. The dashed black lines highlight incised stream reaches that no longer contain water, indicating the streams were formerly through-flowing prior to the formation of the moulin directly upstream. The large blue stream in the foreground is estimated to be 10 m wide. c) Aerial photograph of small stream that appears to be recently bisected by a fracture that caused an offset (black arrow) in the stream trace. The channel on the left appears to be dry. This is likely an early stage in the moulin formation process as there is no obvious moulin visible from above, yet the water from the stream section of the right disappears at the fracture. The stream section on the left is estimated to be 1 m wide.

identification of which moulins likely form as the conduit for a lake drainage event serves two purposes. First, it identifies which moulins do not necessarily require an explanation for their formation, apart from what triggered that lake to drain. Second, it identifies the long-term population of lake drainages within the study area, each of which is assumed to potentially affect the stress field in a similar way to the single lake drainage event that we model.



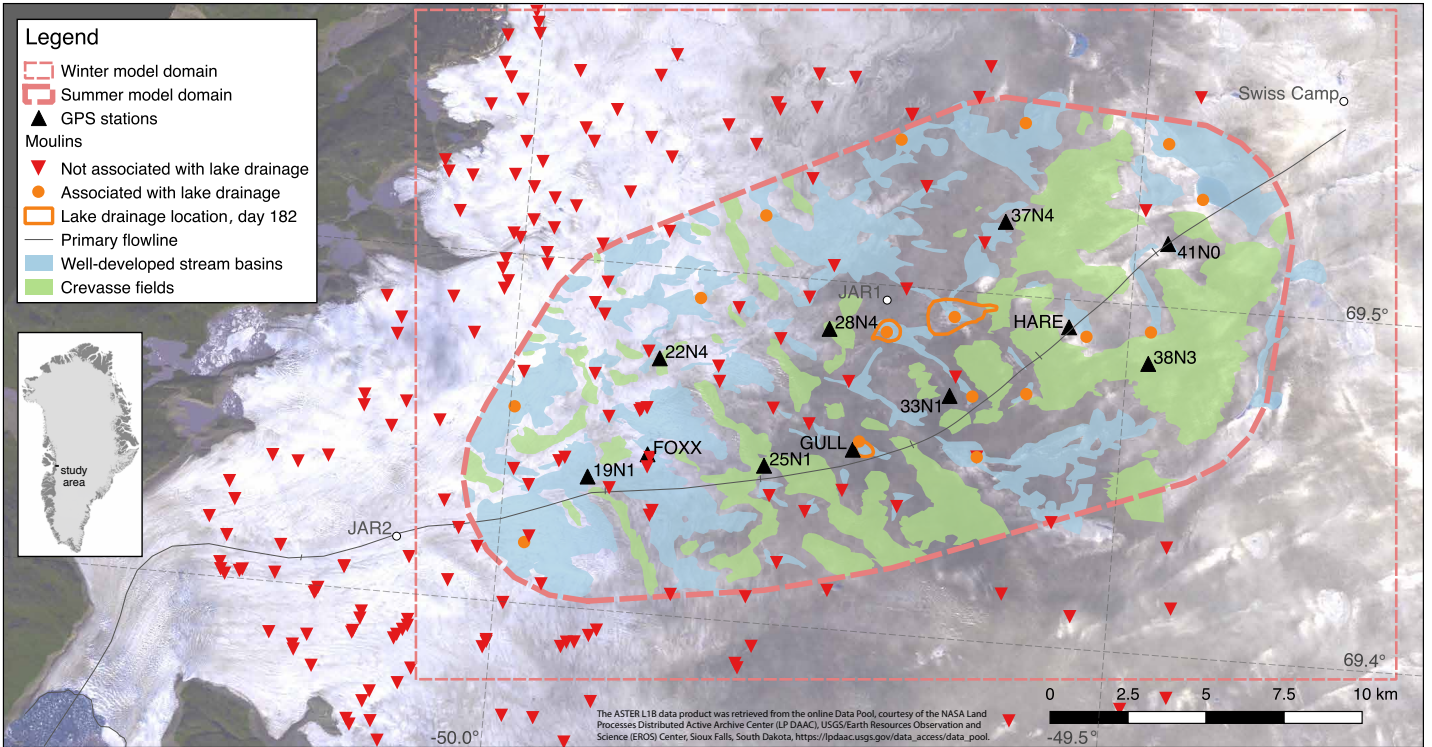


**Figure 2.** Map of study area. Modeled domain boundaries are shown with pink dashed lines. GPS locations are shown as black triangles and labeled with station name. Moulins mapped from satellite imagery are shown as red symbols. Those co-located with lake drainages identified by *Morriss et al.* [2013] within the study area are represented as circles; all others are triangles. The primary flowline of Sermeq Avannarleq is shown as a gray line. Well-developed stream basins that are absent of visible crevasses and mapped from 2 m resolution satellite imagery are shown as light blue areas. Persistent crevasse fields mapped from 2 m resolution satellite imagery are shown in green. See Supporting Figure 2 for derivation of persistent crevasse field locations. The lake drainages on day 182 of 2011 are shown as with orange lines. The background image is from ASTER, acquired July 16, 2010.

## 2.2 Ice Velocity Data

During summer of 2011, we maintained a network of eleven GPS receivers spaced about four ice thicknesses apart across the study area (Figure 2). At each GPS site, we calculated kinematic GPS positions by carrier-phase differential processing [Chen, 1998]. Velocities were calculated using a 6-hour time window following methods discussed in Hoffman et al. [2011], Tedesco et al. [2013], and Andrews et al. [2014]. The resulting product used here is a time-series of ice velocity (two horizontal components) at each receiver site posted at two-hour intervals during periods that all receivers had complete data. This includes a portion of the spring speedup (two short periods during day of year 161.75–164.25) and an eight day period of strong diurnal velocity variations during summer (day of year 178.25–186.58, 27 June to 5 July) (Supporting Figure 4). In the center of this time period, three supraglacial lakes within the network drained on day 182 (Figure 2, Supporting Figure 4) [Morriss et al., 2013], which we refer to collectively as a single “event”. Note that analysis of satellite imagery [Morriss et al., 2013] indicates a total of 20 supraglacial lakes drained in or near our study area in 2011, but no other events are clearly identifiable in the velocity record within the time period used here. We addi-

tionally use a spatially-complete velocity field representative of winter conditions measured from Interferometric Synthetic Aperture Radar (InSAR) by the NASA Making Earth System Data Records for Use in Research Environments (MEaSUREs) program [Joughin *et al.*, 2010] averaged for all available winters (2007-2012).

### 2.3 Ice Sheet Dynamics Inverse Model

We estimate ice stresses during the study period by solving a partial differential equation-constrained optimization problem using the adjoint capabilities of the Albany/FELIX ice sheet model [Perego *et al.*, 2014; Tezaur *et al.*, 2015]. The model solves the three-dimensional, first-order approximation of the Stokes-flow momentum balance [Blatter, 1995; Pattyn, 2003] with a temperature-dependent Glen’s law rheology [Glen, 1955; Cuffey and Paterson, 2010] using the finite element method.

We use the sparse network of GPS-derived velocity measurements with high temporal resolution as control points to solve the ice sheet stress balance inverse problem independently at each time step. Inverse modeling of ice dynamics from observations of surface velocity has become a common tool in glaciology [e.g. Macayeal, 1993; Joughin *et al.*, 2004; Jay-Allemand *et al.*, 2011; Habermann *et al.*, 2012, 2013; Perego *et al.*, 2014; Shapero *et al.*, 2016]. While the sparsity of the GPS observations on each time step reduces constraints on the steady inverse problem, the tradeoff is high temporal resolution provided by the high frequency GPS measurements. Our inversion method is based on that described in detail by Perego *et al.* [2014]. It optimizes a basal friction parameter,  $\beta$ , to minimize an objective functional,  $\mathcal{J}$ , which accounts for the mismatch between the modeled and observed surface velocity (transformed by the arcsinh function to prevent regions of fast velocity from dominating the cost functional [Perego *et al.*, 2014]) while penalizing sharp gradients in  $\beta$  through Tikhonov regularization. The objective functional,  $\mathcal{J}$ , is defined as

$$\mathcal{J}(\beta) = \frac{1}{2|\Sigma|} \sum_{i=1}^2 \int_{\Sigma} \left( \operatorname{arcsinh} \left( \frac{u_i}{\sigma_{u_i}} \right) - \operatorname{arcsinh} \left( \frac{u_i^{obs}}{\sigma_{u_i}} \right) \right)^2 ds + \frac{\alpha}{2|\Sigma|} \int_{\Sigma} |\nabla \beta|^2 ds, \quad (1)$$

which is defined on the two-dimensional domain  $\Sigma$ , where  $\mathbf{u}$  is the surface velocity,  $\sigma_u$  is (spatially-varying) uncertainty in the observed velocity,  $\alpha$  is the regularization parameter, and  $ds$  indicates spatial integration. We use a linear basal friction law that relates the basal friction parameter,  $\beta(x, y)$ , to the basal traction,  $\tau_b$ , and the sliding velocity,  $\mathbf{u}_b$ :

$$\tau_b = -\beta \mathbf{u}_b. \quad (2)$$

For a given model geometry, ice temperature, boundary conditions,  $\mathbf{u}^{obs}$ ,  $\sigma_u$ , and  $\alpha$ , the inverse model determines the optimal  $\beta$  field, from which the associated three-dimensional velocity and stress fields are inferred.

The two-dimensional model domain  $\Sigma$  is defined by the convex hull of the GPS receiver locations with a 2.5 km buffer (Figure 2). Along the lateral boundaries of the domain, we apply homogeneous Neumann boundary conditions (normal component of the membrane stress is zero). The model uses a spatially-uniform horizontal grid resolution of 500 m and ten evenly-spaced vertical levels, and the velocity and inferred stress fields we discuss below are assumed to have this same resolution. Surface elevation is derived from the Greenland Ice Mapping Project [Howat *et al.*, 2014] and bed elevation is from a mass-conserving bed product described in Supporting Text S1 [Ettema *et al.*, 2009; Joughin *et al.*, 2010; Morlighem *et al.*, 2011; Logg *et al.*, 2012; CReSIS Digital Media, 2012; Morlighem *et al.*, 2013; Brinkerhoff and Johnson, 2015]. Because the small changes in ice thickness over the short time period (weeks) considered here will have a negligible impact on the model solution, ice thickness is held steady in time. Ice temperature for calculating the flow rate parameter required by the ice sheet model is interpolated from borehole temperatures profiles at three locations in the study area [Thomsen *et al.*, 1991;

Lüthi et al., 2015] (Supporting Figure 5). The value for  $\alpha$  is chosen through a so-called L-curve analysis described in Supporting Text S2 [Gillet-Chaulet et al., 2012; Habermann et al., 2012].

The inversion is carried out for each 2-hr time slice in the time-series of GPS point velocity observations, capturing representative time periods for the spring speedup, early summer diurnal velocity variations, and the lake drainage event (Supporting Figure 4). The  $\mathbf{u}^{obs}$  field is defined by the eleven point velocity measurements in the GPS network described above which are interpolated by inverse-distance weighting across the rest of the domain, and  $\sigma_u$  is an empirical function of distance from the nearest GPS station (Supporting Figure 6). An additional inversion is performed using the winter InSAR velocity field [Joughin et al., 2010, 2015] to characterize the winter stress field (Supporting Text S3).

## 2.4 Fracture criterion

Fracturing initiates the formation of both crevasses and moulins; because moulins in west Greenland form through hydrofracture, a prerequisite for moulin formation is a fracture at the ice sheet surface in which water can collect. To identify conditions sufficient for fracture formation, we apply the commonly used von Mises fracture criterion: fracturing occurs when stresses at the glacier surface exceed an observationally-derived tensile strength [Kehle, 1964; Vaughan, 1993; Colgan et al., 2016].

We use the two-hourly, three-dimensional ice stress components output by the ice sheet model to calculate surface parallel principal stresses,  $\sigma_1$  and  $\sigma_2$  [Vaughan, 1993]:

$$\sigma_1 = \sigma_{max} = \frac{1}{2} (\sigma_{xx} + \sigma_{yy}) + \sqrt{\left[ \frac{1}{2} (\sigma_{xx} - \sigma_{yy}) \right]^2 + \tau_{xy}^2} \quad (3)$$

$$\sigma_2 = \sigma_{min} = \frac{1}{2} (\sigma_{xx} + \sigma_{yy}) - \sqrt{\left[ \frac{1}{2} (\sigma_{xx} - \sigma_{yy}) \right]^2 + \tau_{xy}^2}, \quad (4)$$

and the corresponding von Mises stress (maximum octahedral shear stress),  $\sigma_v$ :

$$\sigma_v^2 = \sigma_1^2 + \sigma_2^2 - \sigma_1 \sigma_2. \quad (5)$$

$\sigma_{xx}$  and  $\sigma_{yy}$  are the normal stresses in the x- and y- directions, respectively, at the ice surface, and  $\tau_{xy}$  is the shear stress in the x-y plane at the surface.

Assuming that prevailing stress conditions form persistent crevasse fields, we compare our satellite observations of crevasse extent to modeled stresses from the winter InSAR velocity field to estimate the tensile strength of ice to be 140 kPa in our study area (Supporting Text S3). We then also calculate the summer time series of von Mises stress and compare it with our observations of moulin location to identify the mostly like periods during the seasonal cycle for their formation. In so doing, we assume that the formation of a fracture is the necessary criterion to moulin formation, and that the other criterion of sufficient water supply is satisfied [Boon and Sharp, 2003].

## 3 Results

Results from the series of model inversions clearly demonstrate the effects of seasonal changes and the lake drainage event on stresses at the bed and the surface. Maximum stresses at the ice surface during spring speedup and summer diurnal variations are comparable in magnitude and modestly elevated above winter stresses ( $\sim +50$  kPa for  $\sigma_v$ , Figure 3). We note that our incomplete temporal coverage of the spring speedup (Supporting Figure 4) may cause us to miss the peak stresses during that period. Over the course of a typical day modeled during summer, the inverted basal friction parameter ( $\beta$ ) varies

by a factor of up to four, and corresponding basal traction ( $\tau_b$ ) varies by about  $\pm 15$  kPa (Supporting Movie S1). A reduced basal traction perturbation forms at the downstream end of the study area around midday local time and moves upglacier as the afternoon continues. It is followed by a high basal traction perturbation in the evening that also progresses upglacier. These patterns presumably demonstrate temporal variations in the delivery of surface meltwater to the bed and corresponding changes in basal lubrication.

During the lake drainage event, the perturbations to  $\beta$ ,  $\tau_b$ , and  $\sigma_v$  are at least twice as large as during summer diurnal variations (up to 8x decrease in  $\beta$  and  $-30$  kPa change in  $\tau_b$ , Supporting Movie S1;  $\sim +100$  kPa for  $\sigma_v$ , Figure 3). In contrast to the diurnal variations, these perturbations progress downglacier, after originating at the uppermost lake drainage site near the upstream end of the study area. The patch of substantially reduced basal traction travels downglacier at  $\sim 1$  km  $\text{hr}^{-1}$  ( $\sim 0.3$  m  $\text{s}^{-1}$ ). This is comparable to typical observed jökulhlaup speeds of  $0.6$  to  $2.7$  m  $\text{s}^{-1}$  [Magnusson *et al.*, 2007; Werder and Funk, 2009]. After the wave of low basal traction passes, basal traction is  $5$ - $10$  kPa higher than before the lake drainage for approximately 12h before gradually returning to pre-event values.

At the surface, these variations in basal traction manifest as substantial variations in the magnitude and direction of the surface parallel principal stresses (Eq. 3-4, Supporting Movie S2a) and associated magnitude of the von Mises stress (Eq. 5, Supporting Movie S2b). Identification of the  $140$  kPa threshold in  $\sigma_v$  during different time periods indicates when formation of the 62 moulins mapped in the study area could occur, provided there is sufficient water at the surface (Figure 3). Specifically, we identify moulin locations where the von Mises criterion for fracturing is met during winter, spring speedup, the period of summer diurnal variations, or the lake drainage event. While the von Mises criterion is only sufficient to initiate surface fracturing, we assume that any developed moulins occur in locations where sufficient surface meltwater exists in summer to drive hydrofracture to the bed.

This analysis indicates that only 6% of mapped moulins occur in locations where winter von Mises stress exceeds the tensile strength. Though von Mises stresses are significantly larger during spring speedup and the diurnal varying conditions during summer, these elevated stresses are only substantial enough to facilitate opening of an additional 9-10% of the moulins. In contrast, the much larger stress experienced during the lake drainage event is sufficient to open 63% of the observed moulins. This includes half of the moulins associated with locations where rapid lake drainage has occurred between 2002 and 2011 (Figure 3c). We assess sensitivity of these results to different choices of the tensile strength and the uncertainty introduced by the sparsity of the GPS observations (Supporting Text 4, Supporting Table 1). Accounting for a range of plausible tensile strength values and the uncertainty introduced by the sparsity of the GPS observations, we find that lake drainage is invariably capable of opening substantially more moulins than the other time periods.

## 4 Discussion

To our knowledge, ours is the first effort to assimilate high-temporal (hourly scale) resolution GPS observations into an inverse ice dynamical modeling framework. Previous efforts at time-varying assimilation have used observational time-series with weekly to annual sampling [Amundson *et al.*, 2006; Jay-Allemand *et al.*, 2011; Joughin *et al.*, 2012; Larour *et al.*, 2014; Goldberg *et al.*, 2015; Gillet-Chaulet *et al.*, 2016; Minchew *et al.*, 2017]. However, some of those efforts perform transient assimilation rather than a set of independent, steady inversions as we have done here. Our approach yields estimates of the ice sheet basal conditions and ice stress state at hourly resolution, which reveals details of the impact of summer meltwater-induced speedup on ice sheet dynamics. Basal traction varies by 15% during diurnal cycles of meltwater delivery to the bed, and by more



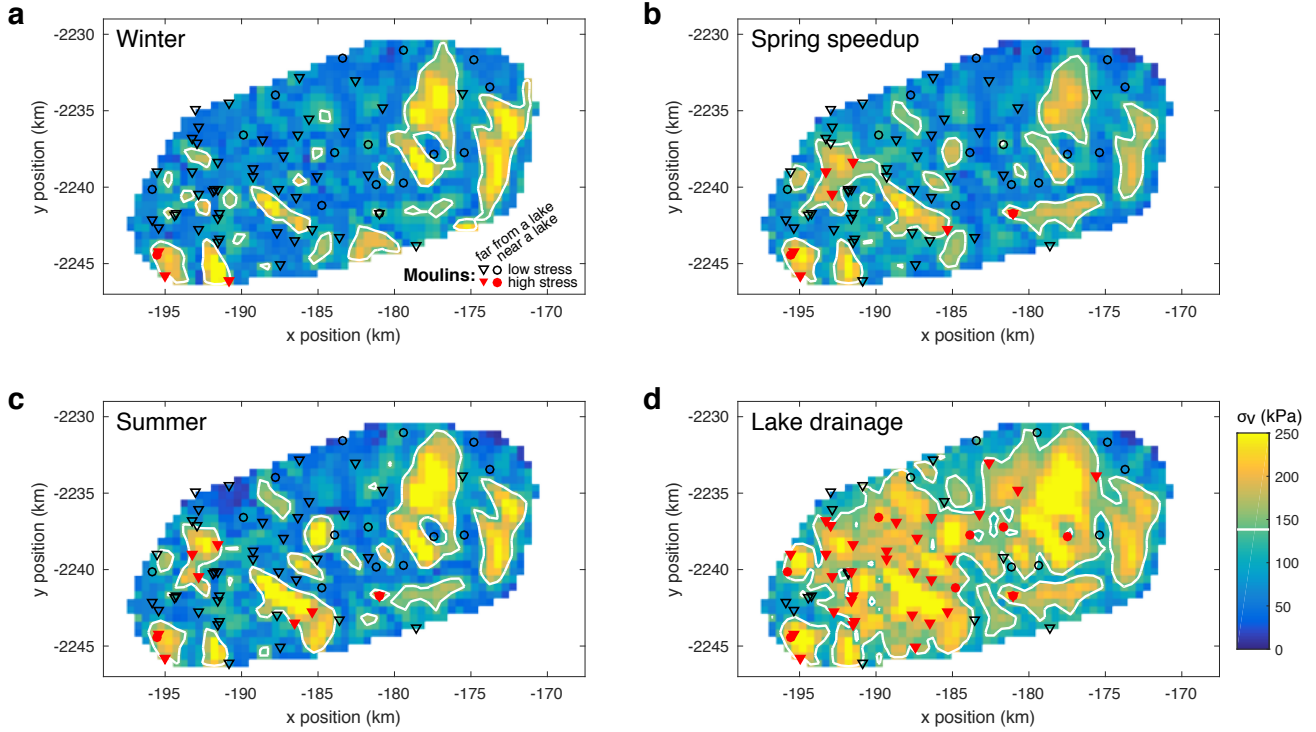


**Figure 3.** Modeled von Mises stress ( $\sigma_v$ ) at different times and mapped moulin locations. a) von Mises stress during winter (prior to day 160). b) Maximum von Mises stress during spring speedup, day 161.75–162.33 (June 10–11) and 164.13–164.25 (June 13). c) Maximum von Mises stress during summer, day 178.25–186.58 (June 27–July 5), excluding 182.2–183.3 (July 1–2). d) Maximum von Mises stress during lake drainage event, days 182.2–183.3 (July 1–2). In each panel, the  $\sigma_v=140$  kPa contour is shown in white. Moulines located in regions of  $\sigma_v < 140$  kPa are shown as open black symbols and those in regions of  $\sigma_v > 140$  kPa are shown as filled red symbols. Moulines co-located with lake drainages identified by *Morriss et al.* [2013] are shown as circles, and all others as triangles. See Supporting Figure 4 for depiction of time periods used.

than twice that during the lake drainage event. After the event, basal traction is 5–10% higher than before it, quantifying the effect of enhanced subglacial drainage efficiency generated during the accommodation of the lake’s volume. This decreased basal lubrication has been inferred previously from GPS measurements [*Das et al.*, 2008; *Hoffman et al.*, 2011; *Doyle et al.*, 2013; *Tedesco et al.*, 2013], modeling of deformation from GPS measurements [*Stevens et al.*, 2015], and proposed based on numerical modeling experiments [*Pimentel and Flowers*, 2010; *Dow et al.*, 2015].

While the use of GPS observations in the ice sheet model inversion provides unique temporal resolution, there is a tradeoff in spatial resolution due to the limited number of observation points, even with a relatively dense GPS network. This sparse coverage provides weak constraints to the optimization problem and necessitates a larger degree of regularization, which smooths the  $\beta$  field to about the typical spacing between GPS stations. This coarse resolution prevents investigation of small scale variations in basal conditions hypothesized to be acting in our study area [*Ryser et al.*, 2014b; *Andrews et al.*, 2014; *Hoffman et al.*, 2016].

#### 4.1 Lake drainage as widespread moulin formation mechanism

We see strong evidence that the majority of moulins exist in locations where the prevailing stress state that occurs over the long winter season is insufficient to support fracturing. Only during the observed lake drainage event are surface stresses sufficient for fracture initiation. We hypothesize that during these transient events, small surface cracks form over large areas, and where the largest such fractures intersect supraglacial streams or lakes, a steady supply of water is able to create a moulin through hydrofracturing (as seen in Figure 1b,c).

Once moulins form, sustained supply of water maintains them through melting and pressure, even after a return to the background stress state otherwise allows transient fractures to close. Moulins are known to last multiple years before being advected away from their sustaining water source [Catania *et al.*, 2008; Catania and Neumann, 2010], meaning that only a fraction of the moulins observed may necessarily form during any given lake drainage event. This suggests these moulins occur by an infrequent process, such as we propose.

The majority of water not flowing into crevasses is drained by lake drainage and the subsequent moulin accommodating continued runoff through the rest of the summer [Koziol *et al.*, 2017]. Stevens *et al.* [2015] described how precursor drainage of surface meltwater routed to a pre-existing moulin near a supraglacial lake caused uplift and longitudinal strain that temporarily perturbed the stress field sufficiently to allow hydrofracture from the ample water supply in the lake and, in turn, rapid lake drainage. Fitzpatrick *et al.* [2014] similarly hypothesized that perturbations to the ice sheet stress field in summer lead to clustering of linked lake drainages, and Boon and Sharp [2003] suggested this to be an important process during hydrofracture on an Arctic glacier.

Our results suggest that cascading hydrofracture events are in fact widespread and apply not just to the formation of moulins beneath lakes, but also to moulins along supraglacial streams. It should be noted that while in our analysis a lake drainage generates stresses sufficient to allow the formation of only 63% of the moulins in our study area, it is only a single, representative lake drainage event. The supraglacial lake inventory by Morriss *et al.* [2013] found 78 lakes within 10 km laterally of the centerline of our study area, 73 of which drained rapidly at least once within a ten year period. Over their ten year record, the majority of rapid lake drainages occur as clusters of multiple lakes draining in a single day (including two additional draining lakes downglacier of our study area and one upglacier on the same day as the three-lake drainage event we model), indicating such a cascading effect of lake drainages may be the norm and not an exception [Fitzpatrick *et al.*, 2014; Williamson *et al.*, 2017]. A common “domino effect” among multiple lake drainages would explain why previous studies have been unsuccessful relating rapid lake drainage occurrence to background variables like ice thickness and water depth [Fitzpatrick *et al.*, 2014; Williamson *et al.*, 2017].

While the formation of moulins occurring beneath lakes or where streams terminate in persistent fractures can readily be explained, many occur away from crevassed regions [Colgan *et al.*, 2011; McGrath *et al.*, 2011; Lampkin and Vanderberg, 2014; Smith *et al.*, 2015] (Figure 2). Koziol *et al.* [2017] estimated that such moulins drain almost half of the water not draining into crevasses in the region of our study area. We propose that such moulins form when transient fractures, formed during the brief, high stresses of a lake drainage event, intersect pre-existing supraglacial streams that then provide sustained water input to the nascent fractures to rapidly facilitate full-thickness hydrofracture. We see ample anecdotal evidence for the moulin development process in various stages along supraglacial streams (Figure 1b,c). Many of the observed moulins occur in regions that have prevailing winter von Mises stress well below the tensile strength (Figure 3a), as evidenced observationally by the absence of crevasse fields and the presence of large, mature supraglacial stream networks (Figure 1b).

## 4.2 Implications of lake-driven moulin formation

Our conclusion that most moulins located away from persistent crevasse fields can only form during rapid supraglacial lake drainage events suggests that these events are a primary control on the number and spacing of moulins across the ice sheet surface. Though these events are relatively infrequent (typically occurring at most once per year per lake) and brief (tens of hours), the ability of moulins to persist multiple years once formed gives the drainage events a long-lived legacy. Moulin density and its impact on where and how much water is delivered to the bed is an important control on subglacial drainage efficiency [Gulley *et al.*, 2012; Banwell *et al.*, 2016] and related ice dynamic response to meltwater basal lubrication. Thus, by triggering the formation of moulins, the impact of lake drainage on ice dynamics and Greenland’s summer speedup is likely to be more extensive than the direct and short-lived speedup following the drainage itself.

There has been concern that surface meltwater-induced speedup of the Greenland Ice Sheet will occur at higher elevations in the future as supraglacial lake drainage at higher elevations opens new moulins there [Liang *et al.*, 2012; Howat *et al.*, 2013; Leeson *et al.*, 2015; Ignézi *et al.*, 2016], potentially leading to increased mass flux towards the ocean and associated sea level rise. Recently, Poinar *et al.* [2015] assess a low likelihood for moulin formation at these higher elevations now and in the future due to low stresses found there. However, our work suggests that should isolated supraglacial lake drainages manage to occur in or near these regions, perhaps due to locally favorable stress conditions or at locations downstream of the low-risk region, they may trigger formation of additional surface-to-bed connections many kilometers away in locations that hold surface water, even if the background stress conditions there are unfavorable to fracturing. This, coupled with a typical moulin lifespan of years [Catania *et al.*, 2008; Catania and Neumann, 2010], could make these areas more vulnerable to surface meltwater reaching the bed than previously thought.

## 5 Conclusions

Using an inverse ice sheet model in a novel configuration forced by a network of high temporal resolution GPS ice velocity observations, we investigated how ice stress conditions relate to fracturing and moulin formation in western Greenland. Comparing an observationally derived tensile strength of ice with modeled stresses during summer, we conclude that 63% the observed moulins in our study area would only experience stress of sufficient magnitude to allow moulin formation during lake drainage events. While previous studies identified the possibility of a cascading effect of meltwater reaching the bed through moulins modifying local stresses to cause supraglacial lake drainage, our results provide direct evidence that this effect can be widespread and act over distances of many kilometers.

Our findings that surface-to-bed connections are primarily created by transient stress conditions during summer indicate that supraglacial lake drainage events are a primary control on moulin density and spatial extent, which, in turn, are known to strongly affect subglacial drainage efficiency. As Greenland runoff and lake drainage frequency is expected to increase in magnitude and elevation range, this process would further increase the number of moulins, potentially mitigating the lubricating effects of additional surface melt reaching the bed in regions where melt currently drains to the bed. However, this also provides a long distance mechanism for opening new moulins at higher elevations that appear otherwise unsusceptible to meltwater-induced acceleration.

## Acknowledgments

This work was supported by a grant to M.J.H. from the Laboratory Directed Research and Development Early Career Research Program at Los Alamos National Laboratory (20160608ECR). Support for M.P. and S.F.P. was provided by the Scientific Discovery through Advanced Computing (SciDAC) program funded by the U.S. Department of Energy, Office of Science, Advanced Scientific Computing Research and Biological and Environmental Research Programs. Sandia National Laboratories is a multimission laboratory managed and operated by National Technology and Engineering Solutions of Sandia, LLC., a wholly owned subsidiary of Honeywell International, Inc., for the U.S. Department of Energy's National Nuclear Security Administration under contract DE-NA-0003525. L.C.A. was supported by an appointment to the NASA Postdoctoral Program at the Goddard Space Flight Center, administered by Universities Space Research Association under contract with NASA, and UTIG Ewing-Worzel and Gale White Graduate Student Fellowships. J.J. was supported by National Science Foundation Office of Polar Programs award 1504457. M.L. was supported by Swiss National Science Foundation grant 200021\_127197. Satellite data access for this work provided by the Polar Geospatial Center under National Science Foundation Office of Polar Programs awards 1043681 and 1559691. We thank Robert Hawley, Claudia Ryser, and Kristin Schild for contributing to the field work that generated data used in this study. We thank Kristin Poinar for discussions on crevasse and moulin development and Blaine Morriss for consultation on the supraglacial lake drainage record. The authors declare no conflicts of interest. The Albany/FELIX model is openly developed and available at <https://github.com/gahansen/Albany>. Model configuration files and pre- and post-processing scripts are available at [https://bitbucket.org/mhoffman/rogue\\_inversion](https://bitbucket.org/mhoffman/rogue_inversion). Observational data and model output are archived at <https://doi.org/10.5281/zenodo.1044471>.

## References

- Amundson, J. M., M. Truffer, and M. P. Luethi (2006), Time-dependent basal stress conditions beneath Black Rapids Glacier, Alaska, USA, inferred from measurements of ice deformation and surface motion, *Journal of Glaciology*, 52(178), 347–357.
- Andrews, L. C., G. A. Catania, M. J. Hoffman, J. D. Gulley, M. P. Lüthi, C. Ryser, R. L. Hawley, and T. A. Neumann (2014), Direct observations of evolving subglacial drainage beneath the Greenland Ice Sheet, *Nature*, 514(7520), 80–83, doi:10.1038/nature13796.
- Arnold, N. S., A. F. Banwell, and I. C. Willis (2014), High-resolution modelling of the seasonal evolution of surface water storage on the Greenland Ice Sheet, *The Cryosphere*, 8(4), 1149–1160, doi:10.5194/tc-8-1149-2014.
- Banwell, A., I. Hewitt, I. Willis, and N. Arnold (2016), Moulin density controls drainage development beneath the Greenland Ice Sheet, *Journal of Geophysical Research Earth Surface*, pp. 2248–2269, doi:10.1002/2015JF003801.
- Banwell, A. F., N. S. Arnold, I. C. Willis, M. Tedesco, and A. P. Ahlstrøm (2012), Modeling supraglacial water routing and lake filling on the Greenland Ice Sheet, *Journal of Geophysical Research*, 117(F4), 1–11, doi:10.1029/2012JF002393.
- Bartholomew, I., P. Nienow, D. Mair, A. Hubbard, M. A. King, and A. Sole (2010), Seasonal evolution of subglacial drainage and acceleration in a Greenland outlet glacier, *Nature Geoscience*, 3, 408–411, doi:10.1038/NGEO863.
- Blatter, H. (1995), Velocity and stress-fields in grounded glaciers - a simple algorithm for including deviatoric stress gradients, *Journal of Glaciology*, 41(138), 333–344.
- Boon, S., and M. Sharp (2003), The role of hydrologically-driven ice fracture in drainage system evolution on an Arctic glacier, *Geophysical Research Letters*, 30(18), 3–6, doi:10.1029/2003GL018034.
- Brinkerhoff, D., and J. Johnson (2015), A stabilized finite element method for calculating balance velocities in ice sheets, *Geoscientific Model Development*, 8(5), 1275–1283, doi:10.5194/gmd-8-1275-2015.

- Carmichael, J. D., I. Joughin, M. D. Behn, S. Das, M. A. King, L. Stevens, and D. Lizarralde (2015), Seismicity on the western Greenland Ice Sheet: Surface fracture in the vicinity of active moulins, *Journal of Geophysical Research F: Earth Surface*, 120(6), 1082–1106, doi:10.1002/2014JF003398.
- Catania, G. A., and T. A. Neumann (2010), Persistent englacial drainage features in the Greenland Ice Sheet, *Geophysical Research Letters*, 37(2), 1–5, doi:10.1029/2009GL041108.
- Catania, G. A., T. A. Neumann, and S. F. Price (2008), Characterizing englacial drainage in the ablation zone of the Greenland ice sheet, *Journal of Glaciology*, 54(187), 567–578.
- Chen, G. (1998), GPS kinematic positioning for airborne laser altimetry at Long Valley, California, Ph.d., Massachusetts Institute of Technology.
- Clason, C. C., D. W. F. Mair, P. W. Nienow, I. D. Bartholomew, A. Sole, S. Palmer, and W. Schwanghart (2015), Modelling the transfer of supraglacial meltwater to the bed of Leverett Glacier, Southwest Greenland, *The Cryosphere*, 9, 123–138, doi:10.5194/tc-9-123-2015.
- Colgan, W., K. Steffen, W. S. Mclamb, W. Abdalati, H. Rajaram, R. Motyka, T. Phillips, and R. Anderson (2011), An increase in crevasse extent, West Greenland: Hydrologic implications, *Geophysical Research Letters*, 38, 1–7, doi:10.1029/2011GL048491.
- Colgan, W., H. Rajaram, W. Abdalati, C. Mccutchan, R. Mottram, M. S. Moussavi, and S. Grigsby (2016), Glacier crevasses: Observations, models, and mass balance implications, *Reviews of Geophysics*, 54, 1–43, doi:10.1002/2015RG000504.Received.
- CRISIS Digital Media (2012), Radar Depth Sounder Data.
- Cuffey, K., and Paterson (2010), *The Physics of Glaciers*, 4th ed., 704 pp., Butterworth-Heinemann, Amsterdam.
- Das, S. B., I. Joughin, M. D. Behn, I. M. Howat, M. A. King, D. Lizarralde, and M. P. Bhatia (2008), Fracture Propagation to the Base of the Greenland Ice Sheet During Supraglacial Lake Drainage, *Science*, 320, 778–781.
- Dow, C. F., B. Kulesa, I. C. Rutt, V. C. Tsai, S. Pimentel, S. H. Doyle, D. As, K. Lindbäck, R. Pettersson, G. A. Jones, and A. Hubbard (2015), Modeling of subglacial hydrological development following rapid supraglacial lake drainage, *Journal of Geophysical Research: Earth Surface*, 120, 1127–1147, doi:10.1002/2014JF003333.
- Doyle, S. H., a. L. Hubbard, C. F. Dow, G. a. Jones, a. Fitzpatrick, a. Gusmeroli, B. Kulesa, K. Lindback, R. Pettersson, and J. E. Box (2013), Ice tectonic deformation during the rapid in situ drainage of a supraglacial lake on the Greenland Ice Sheet, *The Cryosphere*, 7(1), 129–140, doi:10.5194/tc-7-129-2013.
- Ettema, J., M. R. van den Broeke, E. van Meijgaard, W. J. van de Berg, J. L. Bamber, J. E. Box, and R. C. Bales (2009), Higher surface mass balance of the Greenland ice sheet revealed by high-resolution climate modeling, *Geophysical Research Letters*, 36(12), L12,501, doi:10.1029/2009GL038110.
- Fitzpatrick, A. A. W., A. L. Hubbard, J. E. Box, D. J. Quincey, D. van As, A. P. B. Mikkelsen, S. H. Doyle, C. F. Dow, B. Hasholt, and G. A. Jones (2014), A decade (2002–2012) of supraglacial lake volume estimates across Russell Glacier, West Greenland, *The Cryosphere*, 8, 107–121, doi:10.5194/tc-8-107-2014.
- Gillet-Chaulet, F., O. Gagliardini, H. Seddik, M. Nodet, G. Durand, C. Ritz, T. Zwinger, R. Greve, and D. G. Vaughan (2012), Greenland ice sheet contribution to sea-level rise from a new-generation ice-sheet model, *The Cryosphere*, 6(6), 1561–1576, doi:10.5194/tc-6-1561-2012.
- Gillet-Chaulet, F., G. Durand, O. Gagliardini, C. Mosbeux, J. Mouginot, F. Rémy, and C. Ritz (2016), Assimilation of surface velocities between 1996 and 2010 to constrain the form of the basal friction law under Pine Island Glacier, *Geophysical Research Letters*, 43(1), 1–11, doi:10.1002/2016GL069937.
- Glen, J. W. (1955), The Creep of Polycrystalline Ice, *Proceedings of the Royal Society A: Mathematical, Physical and Engineering Sciences*, 228(1175), 519–538, doi:10.1098/

- rspa.1955.0066.
- Goldberg, D. N., P. Heimbach, I. Joughin, and B. Smith (2015), Committed retreat of Smith, Pope, and Kohler Glaciers over the next 30 years inferred by transient model calibration, *The Cryosphere*, 9, 2429–2446, doi:10.5194/tc-9-2429-2015.
- Gulley, J., M. Grabiec, J. Martin, J. Jania, G. Catania, and P. Glowacki (2012), The effect of discrete recharge by moulins and heterogeneity in flow-path efficiency at glacier beds on subglacial hydrology, *Journal of Glaciology*, 58(211), 926–940, doi:10.3189/2012JoG11J189.
- Habermann, M., D. Maxwell, and M. Truffer (2012), Reconstruction of basal properties in ice sheets using iterative inverse methods, *Journal of Glaciology*, 58(210), 795–807, doi:10.3189/2012JoG11J168.
- Habermann, M., M. Truffer, and D. Maxwell (2013), Changing basal conditions during the speed-up of Jakobshavn Isbræ, Greenland, *The Cryosphere*, 7(6), 1679–1692, doi:10.5194/tc-7-1679-2013.
- Hoffman, M. J., G. A. Catania, T. A. Neumann, L. C. Andrews, and J. A. Rumrill (2011), Links between acceleration, melting, and supraglacial lake drainage of the western Greenland Ice Sheet, *Journal of Geophysical Research*, 116(F4), F04,035, doi:10.1029/2010JF001934.
- Hoffman, M. J., A. G. Fountain, and G. E. Liston (2016), Distributed modeling of ablation (1996–2011) and climate sensitivity on the glaciers of Taylor Valley, Antarctica, *Journal of Glaciology*, 62(232), 215–229.
- Howat, I. M., S. de la Peña, J. H. van Angelen, J. T. M. Lenaerts, and M. R. van den Broeke (2013), Expansion of meltwater lakes on the Greenland Ice Sheet, *The Cryosphere*, 7(1), 201–204, doi:10.5194/tc-7-201-2013.
- Howat, I. M., a. Negrete, and B. E. Smith (2014), The Greenland Ice Mapping Project (GIMP) land classification and surface elevation data sets, *The Cryosphere*, 8(4), 1509–1518, doi:10.5194/tc-8-1509-2014.
- Ignéczi, Á., A. J. Sole, S. J. Livingstone, A. Leeson, X. Fettweis, N. Selmes, N. Gourmelon, and K. Briggs (2016), North-east sector of the Greenland Ice Sheet to undergo the greatest inland expansion of supraglacial lakes during the 21st century, *Geophysical Research Letters*, pp. 9729–9738, doi:10.1002/2016GL070338.
- Jay-Allemand, M., F. Gillet-Chaulet, O. Gagliardini, and M. Nodet (2011), Investigating changes in basal conditions of Variegated Glacier prior to and during its 1982–1983 surge, *The Cryosphere*, 5(3), 659–672, doi:10.5194/tc-5-659-2011.
- Joughin, I., D. R. MacAyeal, and S. Tulaczyk (2004), Basal shear stress of the Ross ice streams from control method inversions, *Journal of Geophysical Research B: Solid Earth*, 109(9), 1–20, doi:10.1029/2003JB002960.
- Joughin, I., B. E. Smith, I. M. Howat, T. Scambos, and T. Moon (2010), Greenland flow variability from ice-sheet-wide velocity mapping, *Journal of Glaciology*, 56(197), 415–430, doi:10.3189/002214310792447734.
- Joughin, I., B. E. Smith, I. M. Howat, D. Floricioiu, R. B. Alley, M. Truffer, and M. Fahnestock (2012), Seasonal to decadal scale variations in the surface velocity of Jakobshavn Isbrae, Greenland: Observation and model-based analysis, *Journal of Geophysical Research*, 117(F2), F02,030, doi:10.1029/2011JF002110.
- Joughin, I., B. Smith, I. Howat, and T. Scambos (2015), MEaSUREs Multi-year Greenland Ice Sheet Velocity Mosaic, Version 2, *Tech. rep.*, NASA National Snow and Ice Data Distributed Active Archive Center, Boulder, Colorado USA, doi:http://dx.doi.org/10.5067/OC7B04ZM9G6Q.
- Kehle, R. O. (1964), Deformation of the Ross Ice Shelf, Antarctica, *GSA Bulletin*, 75(4), 259–286.
- Koziol, C., N. Arnold, A. Pope, and W. Colgan (2017), Quantifying supraglacial meltwater pathways in the Paakitsoq region, West Greenland, *Journal of Glaciology*, 63(239), 464–476, doi:10.1017/jog.2017.5.



- Krawczynski, M. J., M. D. Behn, S. B. Das, and I. Joughin (2009), Constraints on the lake volume required for hydro-fracture through ice sheets, *Geophysical Research Letters*, 36(10), 1–5, doi:10.1029/2008GL036765.
- Lampkin, D. J., and J. Vanderberg (2014), Supraglacial melt channel networks in the Jakobshavn Isbrae region during the 2007 melt season, *Hydrological Processes*, 28(November 2013), 6038–6053, doi:10.1002/hyp.10085.
- Larour, E., J. Utke, B. Csatho, A. Schenk, H. Seroussi, M. Morlighem, E. Rignot, N. Schlegel, and A. Khazendar (2014), Inferred basal friction and surface mass balance of the Northeast Greenland Ice Stream using data assimilation of ICESat (Ice Cloud and land Elevation Satellite) surface altimetry and ISSM (Ice Sheet System Model), *The Cryosphere*, 8, 2335–2351, doi:10.5194/tc-8-2335-2014.
- Leeson, A. A., A. Shepherd, K. Briggs, I. Howat, X. Fettweis, M. Morlighem, and E. Rignot (2015), Supraglacial lakes on the Greenland ice sheet advance inland under warming climate, *Nature Climate Change*, 5(December 2014), 51–55, doi:10.1038/NCLIMATE2463.
- Liang, Y.-L., W. Colgan, Q. Lv, K. Steffen, W. Abdalati, J. Stroeve, D. Gallaher, and N. Bayou (2012), A decadal investigation of supraglacial lakes in West Greenland using a fully automatic detection and tracking algorithm, *Remote Sensing of Environment*, 123, 127–138, doi:10.1016/j.rse.2012.03.020.
- Logg, A., K.-A. Mardal, and G. Wells (Eds.) (2012), *Automated Solution of Differential Equations by the Finite Element Method*, 731 pp., Springer-Verlag, Berlin, doi:10.1007/978-3-642-23099-8.
- Lüthi, M. P., C. Ryser, L. C. Andrews, G. A. Catania, M. Funk, R. L. Hawley, M. J. Hoffman, and T. Neumann (2015), Heat sources within the Greenland Ice Sheet: dissipation, temperate paleo-firn and cryo-hydrologic warming, *The Cryosphere*, 9, 245–253, doi:10.5194/tc-9-245-2015.
- Macayeal, D. R. (1993), A tutorial on the use of control methods in ice-sheet modeling, *Journal of Glaciology*, 39(131), 91–98.
- Magnusson, E., H. Rott, H. Björnsson, and F. Pálsson (2007), The impact of jokulhlaups on basal sliding observed by SAR interferometry on Vatnajökull, Iceland, *Journal of Glaciology*, 53(181), 232–240, doi:10.3189/172756507782202810.
- McGrath, D., W. Colgan, K. Steffen, P. Lauffenburger, and J. Balog (2011), Assessing the summer water budget of a moulin basin in the Sermeq Avannarleq ablation region, Greenland ice sheet, *Journal of Glaciology*, 57(205), 954–964, doi:10.3189/002214311798043735.
- Minchew, B., M. Simons, H. Björnsson, F. Pálsson, M. Morlighem, H. Seroussi, E. Larour, and S. Hensley (2017), Plastic bed beneath Hofsjökull Ice Cap, central Iceland, and the sensitivity of ice flow to surface meltwater flux, *Journal of Glaciology*, 62(2016), 147–158, doi:10.1017/jog.2016.26.
- Morlighem, M., E. Rignot, H. Seroussi, E. Larour, H. Ben Dhia, and D. Aubry (2011), A mass conservation approach for mapping glacier ice thickness, *Geophysical Research Letters*, 38(19), L19,503, doi:10.1029/2011GL048659.
- Morlighem, M., E. Rignot, J. Mouginot, X. Wu, H. Seroussi, E. Larour, and J. Paden (2013), High-resolution bed topography mapping of Russell Glacier, Greenland, inferred from Operation IceBridge data, *Journal of Glaciology*, 59(218), 1015–1023, doi:10.3189/2013JoG12J235.
- Morriss, B. F., R. L. Hawley, J. W. Chipman, L. C. Andrews, G. a. Catania, M. J. Hoffman, M. P. Lüthi, and T. a. Neumann (2013), A ten-year record of supraglacial lake evolution and rapid drainage in West Greenland using an automated processing algorithm for multispectral imagery, *The Cryosphere*, 7(6), 1869–1877, doi:10.5194/tc-7-1869-2013.
- Pattyn, F. (2003), A new three-dimensional higher-order thermomechanical ice sheet model: Basic sensitivity, ice stream development, and ice flow across subglacial lakes, *Journal of Geophysical Research*, 108(B8), 1–15, doi:10.1029/2002JB002329.

- Perego, M., S. Price, and G. Stadler (2014), Optimal initial conditions for coupling ice sheet models to Earth system models, *Journal of Geophysical Research Earth Surface*, *119*, 1–24, doi:10.1002/2014JF003181.Received.
- Phillips, T., S. Leyk, H. Rajaram, W. Colgan, W. Abdalati, D. Mcgrath, and K. Steffen (2011), Modeling moulin distribution on Sermeq Avannarleq glacier using ASTER and WorldView imagery and fuzzy set theory, *Remote Sensing of Environment*, *115*(9), 2292–2301, doi:10.1016/j.rse.2011.04.029.
- Pimentel, S., and G. E. Flowers (2010), A numerical study of hydrologically driven glacier dynamics and subglacial flooding, *Proceedings of the Royal Society A: Mathematical, Physical and Engineering Sciences*, *467*(2126), 537–558, doi:10.1098/rspa.2010.0211.
- Poinar, K., I. Joughin, S. B. Das, M. D. Behn, J. T. M. Lenaerts, and M. R. Broeke (2015), Limits to future expansion of surface-melt-enhanced ice flow into the interior of western Greenland, *Geophysical Research Letters*, *42*, 1800–1807, doi:10.1002/2015GL063192.Received.
- Poinar, K., I. Joughin, J. T. Lenaerts, and M. R. Van Den Broeke (2017), Englacial latent-heat transfer has limited influence on seaward ice flux in western Greenland, *Journal of Glaciology*, *63*(237), 1–16, doi:10.1017/jog.2016.103.
- Röösli, C., A. Helmstetter, F. Walter, and E. Kissling (2016), Meltwater influences on deep stick-slip icequakes near the base of the Greenland Ice Sheet, *Journal of Geophysical Research: Earth Surface*, *121*, 1–18, doi:10.1002/2015JF003601.
- Ryser, C., M. P. Lüthi, L. C. Andrews, M. J. Hoffman, G. A. Catania, R. L. Hawley, T. A. Neumann, and S. S. Kristensen (2014a), Sustained high basal motion of the Greenland ice sheet revealed by borehole deformation, *Journal of Glaciology*, *60*(222), 647–660, doi:10.3189/2014JoG13J196.
- Ryser, C., M. P. Lüthi, L. C. Andrews, G. A. Catania, M. Funk, R. Hawley, M. Hoffman, and T. Neumann (2014b), Caterpillar-like ice motion in the ablation zone of the Greenland ice sheet, *Journal of Geophysical Research: Earth Surface*, *119*(10), 1–14, doi:10.1002/2013JF003067.
- Shapero, D. R., I. R. Joughin, K. Poinar, M. Morlighem, and F. Gillet-chaulet (2016), Basal resistance for three of the largest Greenland outlet glaciers, *Journal of Geophysical Research: Earth Surface*, *121*, 168–180, doi:10.1002/2015JF003643.Resistance.
- Smith, L. C., V. W. Chu, K. Yang, C. J. Gleason, L. H. Pitcher, A. K. Rennermalm, C. J. Legleiter, A. E. Behar, B. T. Overstreet, S. E. Moustafa, M. Tedesco, R. R. Forster, A. L. LeWinter, D. C. Finnegan, Y. Sheng, and J. Balog (2015), Efficient meltwater drainage through supraglacial streams and rivers on the southwest Greenland ice sheet, *Proceedings of the National Academy of Sciences*, *112*(4), 1001–1006, doi:10.1073/pnas.1413024112.
- Stevens, L. a., M. D. Behn, J. J. McGuire, S. B. Das, I. Joughin, T. Herring, D. E. Shean, and M. a. King (2015), Greenland supraglacial lake drainages triggered by hydrologically induced basal slip, *Nature*, *522*(7554), 73–76, doi:10.1038/nature14480.
- Tedesco, M., I. Willis, M. Hoffman, A. Banwell, P. Alexander, and N. Arnold (2013), Ice dynamic response to two modes of surface lake drainage on the Greenland Ice Sheet, *Environmental Research Letters*, *8*, 034,007 (9pp), doi:10.1088/1748-9326/8/3/034007.
- Tezaur, I. K., M. Perego, A. G. Salinger, R. S. Tuminaro, and S. Price (2015), Albany/FELIX: a parallel, scalable and robust, finite element, first-order Stokes approximation ice sheet solver built for advanced analysis, *Geoscientific Model Development*, *8*, 1–24, doi:10.5194/gmd-8-1-2015.
- Thomsen, H., O. Olesen, R. J. Braithwaite, and C. E. Boggild (1991), Ice drilling and mass balance at Pakitsq, Jakobshavn, central West Greenland, Report 152., *Tech. rep.*, Grønlands Geologiske Undersøgelse, Copenhagen, Denmark.
- Tsai, V. C., and J. R. Rice (2010), A model for turbulent hydraulic fracture and application to crack propagation at glacier beds, *Journal of Geophysical Research*, *115*(F3), doi:10.1029/2009JF001474.

- van der Veen, C. J. (2007), Fracture propagation as means of rapidly transferring surface meltwater to the base of glaciers, *Geophysical Research Letters*, *34*(1), 1–5, doi:10.1029/2006GL028385.
- Vaughan, D. G. (1993), Relating the occurrence of crevasses to surface strain rates, *Journal of Glaciology*, *39*(132), 255–266, doi:10.1016/0148-9062(94)90888-5.
- Walter, F., J. Chaput, and M. P. Luthi (2014), Thick sediments beneath Greenland's ablation zone and their potential role in future ice sheet dynamics, *Geology*, *42*(6), 487–490, doi:10.1130/G35492.1.
- Werder, M. A., and M. Funk (2009), Dye tracing a jokulhlaup: II. Testing a jokulhlaup model against flow speeds inferred from measurements, *J. Glaciol.*, *55*(193)(193), 899–908.
- Williamson, A. G., N. S. Arnold, A. F. Banwell, and I. C. Willis (2017), A Fully Automated Supraglacial lake area and volume Tracking ("FAST") algorithm: Development and application using MODIS imagery of West Greenland, *Remote Sensing of Environment*, *196*, 113–133, doi:10.1016/j.rse.2017.04.032.
- Yang, K., and L. C. Smith (2016), Internally drained catchments dominate supraglacial hydrology of the southwest Greenland Ice Sheet, *Journal of Geophysical Research: Earth Surface*, *121*, 1891–1910, doi:10.1002/2016JF003927. Received.
- Zwally, H. J., W. Abdalati, T. Herring, K. Larson, J. Saba, and K. Steffen (2002), Surface melt-induced acceleration of Greenland ice-sheet flow., *Science*, *297*(5579), 218–22, doi:10.1126/science.1072708.